Article

Imaging catalysis: Operando investigation of the CO2 hydrogenation reaction dynamics by means of infrared thermography

Robin Mutschler, Emanuele Moioli, Kun Zhao, Loris Lombardo, Emad Oveisi, Alessandro Porta, Leonardo Falbo, Carlo Giorgio Visconti, Luca Lietti, and Andreas Zuttel

ACS Catal., **Just Accepted Manuscript** • DOI: 10.1021/acscatal.9b04475 • Publication Date (Web): 11 Dec 2019

Imaging catalysis: Operando investigation of the CO_2 hydrogenation reaction dynamics by means of infrared thermography

Robin Mutschler[a,b,*], Emanuele Moioli[a,b.*], Kun Zhao[a,b], Loris Lombardo[a,b], Emad Oveisi[c], Alessandro Porta[d], Leonardo Falbo[d], Carlo Giorgio Visconti[d], Luca Lietti[d], Andreas Züttel[a,b]

[a]*Laboratory of Materials for Renewable Energy (LMER), Institute of Chemical Sciences and Engineering (ISIC), Basic Science Faculty (SB), École polytechnique fédérale de Lausanne (EPFL) Valais/Wallis, Energypolis, Sion, Switzerland. Rue de l'Industrie 17, CP 440, CH-1951 Sion, Switzerland*

[b]*Empa Materials Science & Technology, CH-8600 Dübendorf, Switzerland*

[c] *Interdisciplinary Centre for Electron Microscopy (CIME), École Polytechnique Fédérale de Lausanne (EPFL), CH-1015 Lausanne, Switzerland*

[d]*Dipartimento di Energia, Politecnico Di Milano, via Lambruschini 4, Milano, 20156, Italy*

**robin.mutschler@epfl.ch*

**emanuele.moioli@epfl.ch*

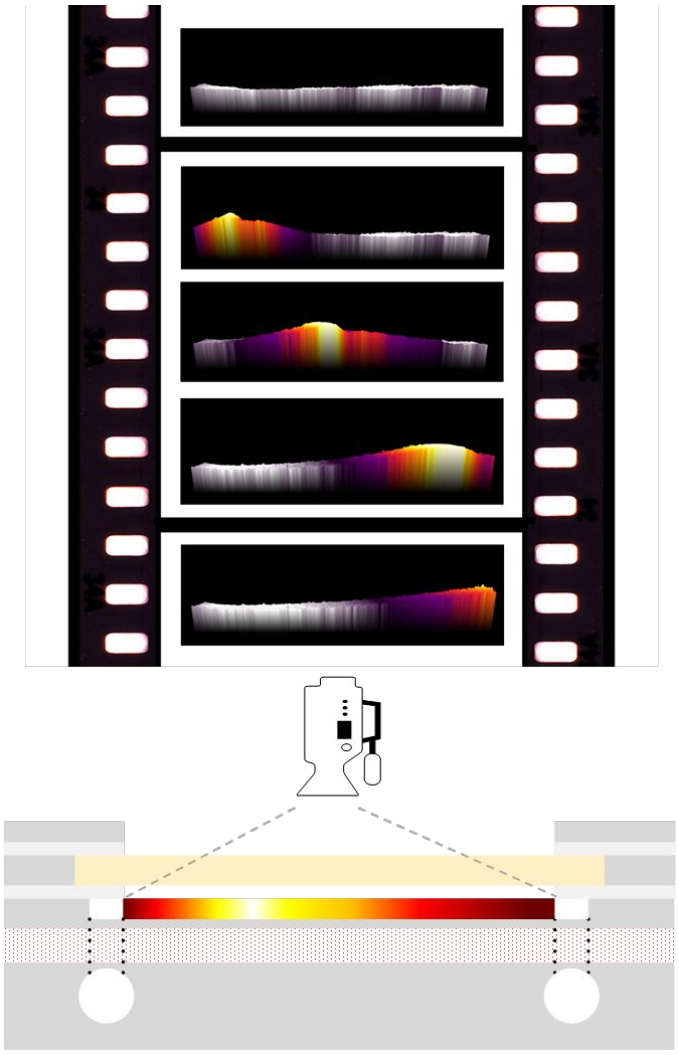

1. Abstract

Infrared thermography is a powerful tool to investigate the dynamic evolution of temperature in chemical reactions. The CO_2 hydrogenation reaction is an ideal model reaction to assess the presented technique due to its high exothermicity. Various dynamic experiments are performed in a newly designed reaction cell with an infrared transmitting ZnSe window. In particular, the gas exchange reactions between CO_2 and H_2, co-injection of the two reactants and the study of the effect of inert gas addition is investigated. Here we show that the reaction rate on the surface of a catalyst can be localized in time and space by means of infrared thermography. This opens the way to the precise description of reaction dynamics, in particular for reactions operating in intermitting conditions. Furthermore, we show that the combination of infrared thermography with other analytic techniques such as rapid and quantitative mass spectrometry enables a holistic understanding of the transient reaction phenomena.

Keywords: IR thermography, CO_2 methanation, catalyst reduction, transient kinetics, operando spectroscopy, heterogeneous catalysis

2. Introduction

The techniques for the measurement of temperature have roots in medical applications. In particular, contactless and non-invasive infrared (IR) thermography technologies developed significantly since their first applications in the middle of the last century[1]. Today, IR thermography is a versatile technique with high spatial resolutions (over 5 megapixels) and fast acquisition times (sampling rates of over 600Hz), besides enabling contactless temperature measurements. These are the main advantages of IR thermography, making it a more effective measurement method than the use of an array of thermocouples. The main limitation of IR thermography the limited penetration of the radiation in reaction media, limiting the application to the measurement of the surface temperature of an object. This means that the method cannot be applied, for example, to investigate the internal temperature of a living being or a technical device such as a plug flow reactor. Commercial applications of the IR thermography are among others in medicine, infrastructure assessment and inspection of electronic components.

In catalysis, thermography has been applied for the simultaneous screening of catalyst libraries to determine the activity of different catalysts in parallel[2–6]. In the CO_2 and CO methanation reactions thermography was used under steady-state reaction conditions to determine the temperature profile along the catalyst bed[7–9], to investigate the influence of sulphur poisoning of a nickel catalyst[10] and to study the possibilities for process intensification [11]. Furthermore, it was employed for the study of the in situ heat production in open cell foam catalysts for the CO_2 methanation reaction[12]. Further applications are the determination of hot zones in the CO oxidation reaction in catalyst beds for mobile applications or the determination of heat of adsorption[13], the measurement of the enthalpy of reactions[14],the determination of the acidity of solutions via a temperature increase to acidity correlation[15]. Thermography is furthermore applied for the analysis of various other chemical reactions [16–19].

However, while thermography is an established technique under steady-state conditions, a study focusing on the localized and time resolved rate of reaction by means of thermography coupled with rapid gas analysis techniques is still lacking in literature.

Accordingly, the aim of this work was to investigate the transient reaction behaviour between H_2 and CO_2 on a 2 wt.% Ru/Al_2O_3 catalyst by means of operando infrared thermography combined with rapid and quantitative mass spectrometry (MS). The investigations are further supported with surface studies by means of diffuse reflectance infrared Fourier transform spectroscopy (DRIFTS). To carry out the experiments, a dedicated reaction cell with an infrared transmitting Zinc Selenide (ZnSe) window has been developed and manufactured.

This work reveals how operando thermography combined with mass spectrometry enables the correlation of the thermal reaction profile with the product formation for the reaction of H_2 and CO_2 on a Ru/Al_2O_3 catalyst. This leads to a deeper understanding of the reaction activation process and the determination of the localized rate of reaction which depends on different reaction conditions. The results show the significant dependence of the reaction activation dynamics on the initial surface condition and on the injected gas composition. The presented method can be applied to understand the transient reaction behaviour of any endo or exothermic reaction with a focus in optimizing the transient reaction behaviour which is of significance for reactors operating in intermittent conditions. An example would be a reactor for the CO_2 hydrogenation coupled with a (renewable) intermitting heat and H_2 source.

3. Materials and methods

Experimental setup

The reaction cell and the infrared camera are integrated into a dedicated gas controlling and analysis system, which consists of three mass flow controllers which are calibrated for CO_2, H_2 and He and can be operated for flows between 0.4-20 ml/min. Furthermore, the system consists of a Jumo Imago 500 controller, with which the reaction cell and the heating cartridge and the heating rope temperatures are controlled. A dedicated reaction cell with an IR-transparent window has been designed and built for the in operando thermal investigation of reactions. The layout is based on a standard reactor setup for the investigation of the CO_2 hydrogenation reaction[20] and has been modified to fit the IR reaction cell. The layout of the reaction setup with the integrated IR cell and camera are given in Figure S1. Furthermore, the details of the reaction cell, the IR camera, the MS and the catalysts used are given below.

Reaction cell

The reaction cell, as shown in Figure 1Figure 1, is manufactured from Aluminium and is 60 mm long, 40 mm wide and 30 mm high. The catalyst bed has a length of 32 mm, is 6 mm wide and is 1 mm deep. The gas inlets (Swagelok 3 mm connectors) are placed on the side of the reactor, to enable heating and temperature measurement of the reactor cell directly underneath the catalyst bed. The heating cartridge (Maxiwatt, Spain) was selected in its dimensions to cover the full length and width of the catalyst bed. It has a diameter of 6mm, a length of 60mm and a maximal power output of 250 W. To prevent a feedback loop between the background heating of the catalyst bed and the heat from the reaction, the background temperature is set via a fixed power output to the heating cartridge with a Jumo Imago 500 controller. The background temperature can vary within 1K due to the heating cycles of the controller (sinusoidal wave shape, visible during experiments with low heat production). The reference temperature in the reactor cell is measured with a K-type thermocouple which is inserted to a channel in direct vicinity of the heating cartridge directly under the catalyst bed (see Figure S1). For the infrared transmitting window, a polished Zinc Selenide window (41 x 23 x 4 mm) was selected due to its constant transmissivity of around 72% between 2.5 and 14 micrometre wavelengths and its high resistivity to thermal shocks and chemical inertness in most environments (CRYSTRAN LTD, UK). PTFE (1 mm) is used to seal the glass-metal connection. The catalyst bed is 1 mm thick and is levelized with the reactor floor. The distance between the catalyst bed surface and the glass is therefore given by the thickness of the PTFE foil which is approximatively 1mm. The gas inlet and outlet channels are filled with glass wool to ensure that no catalyst powder is transported into the gas lines. Figure 1 below shows the reaction cell and the experimental layout with IR camera. The void space in the catalyst bed is given by the space between the surface of the catalyst and the ZnSe window and the void fraction of the catalyst grains packed to levelize with the reaction cell floor. For the catalyst grains, we assume a random loose packing and therefore approximate the void fraction with 0.4. The gas volume in the catalyst bed is calculated to be 0.27 ml. The space velocity in the reactor is given by the gas flow and the void space of the reaction chamber. As a reference: at a flow of 10 ml/min, the space velocity is 2600 h^{-1}, which corresponds to an average residence time of 1.4 s.

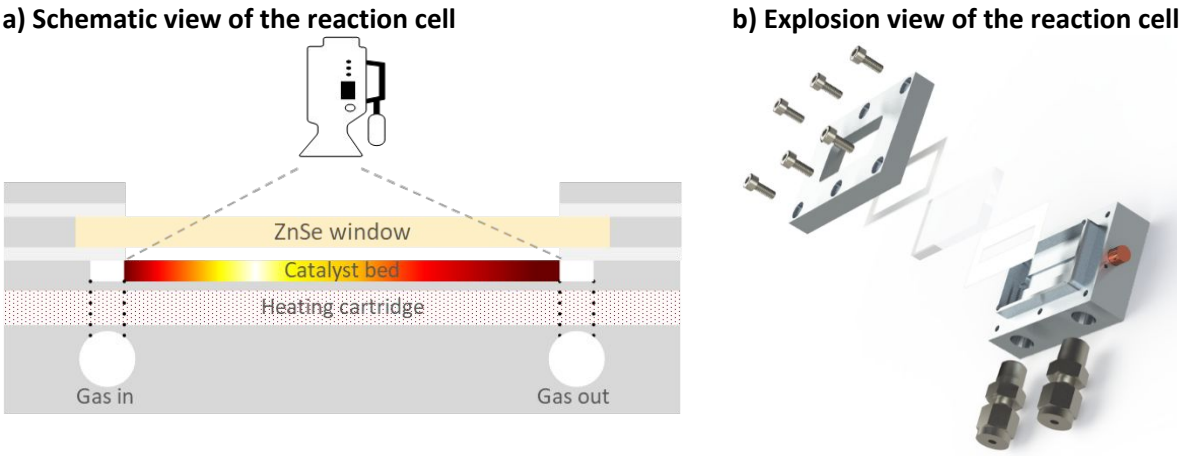

Figure 1: Reaction cell for the in-operando investigation of the heterogeneously catalysed reaction between H_2 and CO_2. a) rendering scheme of the assembled cell with the Aluminium body in dark grey and the PTFE in light grey. The heating cartridge is placed directly underneath the catalyst bed. The voids at the end of the catalyst bed are filled with glass wool to avoid catalyst movement into tubing b) explosion view with the building elements which are from left to right: cap, PTFE sealing, ZnSe window (4 mm), PTFE sealing, reaction bed with heating cartridge (copper) and Swagelok connectors (dark grey metallic).

Thermography camera

The thermal images were recorded with an InfraTec VarioCAM® hr camera, which has a spectral range between 7.5-14 micrometres wavelength. Thermal images were recorded with 50 Hz and a resolution of 640x480 pixels. The camera was equipped with a macro-lens, which results in an effective view field of 21x16mm, corresponding to a pixel side length of 33 micrometres. The expected error in the temperature measurement above 100°C is less than 1K. The camera is directly connected and controlled with a computer and operated through the IRBIS 3.1 pro software from InfraTec. The thermographs of the experiments are acquired and analysed in the InfraTec IRBIS 3.1 plus software. The calibration of the IR camera was carried out with an applied He flow of 10ml/min from room temperature (25.7°C) to elevated temperature (up to 280°C). As stated above, the transmissivity of the 4mm thick Zinc Selenide window is 72%. This value was set in the IRBIS software to determine the emissivity of the reduced 2 wt. % Ru/Al_2O_3 catalyst. The emissivity was found to be 85% by correlating the measured IR-camera temperature to the known ambient temperature of 25.7°C. The temperature measurement of the IR camera and the thermocouple which is directly placed underneath the catalyst bed (See Figure S1) have been tested up to 280°C and deviations of less than 1K have been recorded.

Catalyst

172mg of a 2 wt.% Ru catalyst supported on Al_2O_3 are used in all of the experiments. This catalysts exhibits a high activity for the conversion of CO_2 and H_2 with a high selectivity to CH_4[21–26]. The catalyst was synthesized by means of wet impregnation of the Ru precursor, $Ru(NO)(NO_3)_3$, on γ-Al_2O_3 with an average particle size of 100 µm. The impregnation process was repeated several times to reach the metal loading of 2%. After each impregnation step, the sample was dried overnight at 120°C. The catalyst was activated at 280°C with an H_2 flow of 20ml/min (A complete reduction of $Ru(NO)(NO_3)_3$ occurs at temperatures above 200°C, as shown in Figure S3). The catalyst was characterized by means of XRD (Bruker Discovery 8) and scanning transmission electron microscopy coupled with energy dispersive X-ray spectroscopy (STEM-EDX; FEI Tecnai Osiris, 200kV acceleration voltage) to determine the crystal size, particle size -and

distribution. The crystal size was determined to be approximatively 6nm by means of the Scherrer-Peak width analysis of the XRD pattern (See Figure S6). The crystal size is confirmed by means of STEM. Particle sizes in the range of 6nm to around 25nm were detected. The mean particle size was found to be around 10±2 nm (Figure S7). The particle distribution was determined by analysing high-angle annular dark-field STEM images from three different catalyst areas and are given in the supporting information with the corresponding EDX elemental maps (Figure S8). Further details on the catalyst synthesis, composition, N_2 adsorption isotherm characterization (BET surface area, pore volume, pore diameter), the catalyst activation (TPR), CO_2 adsorption and activation analysis by means of microbalance, crystal size (XRD), particle size and distribution by means of STEM-EDX and the CO_2 desorption and activation energy (TPD) can be found in section 3.8 of the supporting information. Upon oxidation of the reduced catalyst in air over night, an oxide layer of approximatively monolayer thickness forms. The relative calculations and the reasons for this approximation are given in section 3.9 of the SI. Table 1 summarizes the main properties of the Ru/Al_2O_3 catalyst.

Table 1: Main properties of the 2% Ru/Al_2O_3 catalyst

	S_{BET} [m^2g^{-1}]	Ru content [wt.%]	XRD Ru crystal size [nm]	Average Ru particle size [nm]	Major peaks of desorbing CO_2 (TPD) [°C]	CO_2 ads. At 280°C per 1g [mg]
Ru on γ-Al_2O_3 supporting phase	167	2.03	6	10±2	110±10, 390, 510	1.4

Mass spectrometer

A Pfeiffer OmniStar GSD320 mass spectrometer is used for the rapid and quantitative gas analysis of the reaction products. To achieve a sampling speed of 20ms, only the specific mass to charge ratios required for the analysis (m/z 2, 4, 15, 18, 28, 44) of the expected products are sampled (Survey experiments with a scanned spectrum from m/z 1 to m/z 100 have been carried out to support the selection of the specific m/z and make sure no other products than CH_4 (m/z 15) and CO (m/z 28) are present- see section 2 in the SI for further information on catalyst activity over a broad temperature range and the activation energy determination). For the quantification of the partial pressures the general procedure reported in our previous work is followed[20]. The quantitative gas composition analysis is carried out using the Faraday detector of the MS. For the temperature programmed desorption experiments to determine the desorption modes of CO_2 and the activation energy of CO_2 desorption adsorbed at 280°C (Figure S9 and S10), the secondary electron multiplier of the mass spectrometer was applied to achieve a higher sensitivity. Details on the MS measurement procedure and calibration are given in section 4 of the SI.

Experimental procedure

Five different experimental series were carried out for this work by means of the IR-thermography camera coupled with rapid MS analysis. Namely, the surface reduction of the oxidized catalyst, gas exchange reactions between CO_2 and H_2 at three space velocities, the Sabatier reaction at different space velocities, H_2 and CO_2 filled reaction cell and at three different He dilutions. An overview of the experimental series is provided below in Table 2.

Table 2: Overview on experiments discussed in this paper. All experiments are carried out at a base temperature of 280±2°C and a pressure of 1bar.

Experimental series		Inflow gas composition	Initial gas in cell	Inflow [ml/min]	Catalyst pretreatment	Analysis methods	Discussed in manuscript section
1)	**H_2 surface reduction**	H_2	He	20	Oxidized in air over night.	IR, MS	**4.1** 5.1 SI
2)	**Gas exchange reactions**	CO_2	H_2	20 10 5	H_2	IR, MS, DRIFTS	**4.2**, 5.2 SI 5.3 SI
		H_2	CO_2	20 10 5	H_2 →He		
3)	**Undiluted Sabatier reaction**	H_2 and CO_2. Ratio 4:1.	He	20 10 5	H_2→He	IR, MS	**4.3** **4.3.1**
4)	**Diluted Sabatier reaction**	H_2,CO_2 and He. H_2:CO_2 ratio 4:1. He fraction: 25%, 50% and 75%	He	20	H_2→ He	IR, MS	**4.3** **4.3.2** 5.5 SI

DRIFTS measurements

Diffuse reflectance infrared Fourier transform spectroscopy (DRIFTS) measurements are carried out to integrate the information about the phenomena observed by IR thermography and MS and to link them with the occurring surface species. The DRIFTS experiments were carried out in a Bruker Tensor 27 spectrophotometer with a wavenumber resolution of $2cm^{-1}$. In particular, the gas exchange reaction between H_2 and CO_2 were investigated by means of DRIFTS to correlate the phenomena observed in thermography such as the strong retention time in the case of surface covered of carbon surface species upon activation with H_2. All experiments are carried out at a cell temperature of 280°C and a gas flow of 10ml/min. The detailed procedure is explained in section 6 of the SI.

4. Results and discussion

4.1 Reduction of the oxidized catalyst surface

In an initial step, the surface reduction of the oxidized Ru/Al_2O_3 is investigated. The reaction is highly exothermic according to the reaction stoichiometry:

$$2H_2 + O_2^* \rightleftharpoons 2H_2O \qquad \Delta H_r = -483.6 \frac{kJ}{mol} \tag{1}$$

The surface reduction has been investigated on the activated catalyst which was exposed to air overnight. Prior to the reduction, the reaction cell was flushed with helium at 280 °C to eliminate residual gases and moisture. Following that, hydrogen was injected with a volumetric flow of 20ml/min.

It was found that the reaction front creates a hotspot of up to 30K and accelerates continuously through the reactor cell. The temperature increase at a fixed point on the reaction axis is relatively sharp meaning that the temperature reaches the maximum and declines back to the base temperature of 280 °C within approximatively 5s which indicates a rapid reaction completion.

Figure 2a shows the heatmap of the measured temperature in the reaction cell resolved in time and space. The sharp reaction peaks and the wave acceleration (parabolic shape) are clearly visible in this graph. The wave acceleration is due to the increase of reaction rate with temperature, causing a progressive increase in the speed of the reaction front. This acceleration is constant over the reaction cell, as observable in Figure 2b. Here, the linear regression is fitted to 5 measured wave velocities, giving linear plot, as expected for a constantly accelerated motion (the reaction front velocity was experimentally determined at 288°C by analysing the time from one measurement point with known position to the next (Figure S11)). The thermal runaway is the reason for the initial acceleration until the maximal hotspot is reached after approximatively 4s. As it can be seen in Figure 2c, the temperature and water formation (determined by means of MS) approach a quasi-steady state after 5s. Therefore, a further thermal runaway is likely prevented by a limiting factor in the reaction kinetics such as the transport of hydrogen to the surface or the desorption of surface oxygen, which is endothermic[27].

Furthermore, the normalized ratio of H_2O formed and H_2 consumed is plotted in Figure 2c overlapped with the maximal hotspot temperature at the corresponding time (ion current and partial pressures plot of the gas species are given in Figure S12). The detection of the water formed is slightly delayed by approximatively two to three seconds to the decline of H_2. This indicates surface adsorption of the formed water. Furthermore, a delay in the decline of the water formation peak compared to the hotspot evolution is observed. This is likely due to the continuous desorption of water after the reaction front already moved through.

Based on the quantitative mass spectrometry analysis, the partial pressure of water in the product gas stream was determined. From this and from the average particle size and distribution of Ru on the surface, the amount of surface oxygen is calculated to be 1.2×10^{-5} mol which corresponds to a monolayer oxygen surface coverage of the Ru particles. Above 65°C, oxygen desorbs from the Al_2O_3 surface[28] and therefore the oxygen coverage at above 280°C is accounted to the Ru particles only[27]. A detailed calculation on the oxygen coverage of the catalyst surface is given in section 3.9 of the SI. The thin monolayer oxygen coverage explains the rapid surface reduction reaction.

a) Heatmap of the catalyst surface reduction

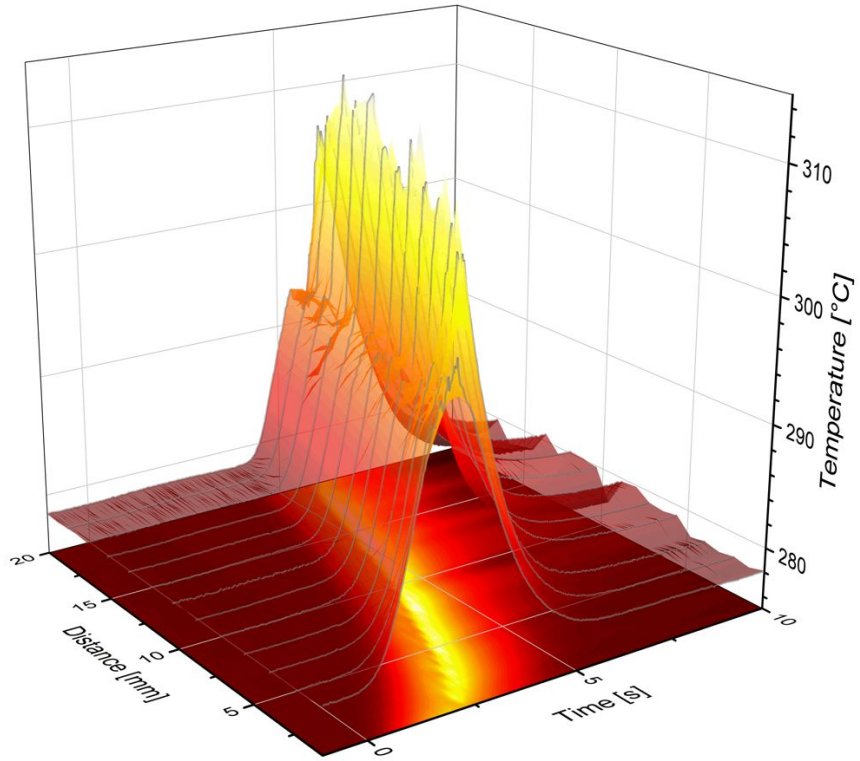

b) Reaction front acceleration

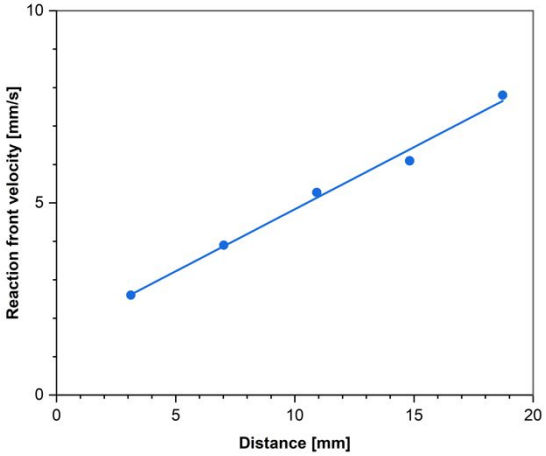

c) Hydrogen consumption and water formation overlapped with maximal wave temperature

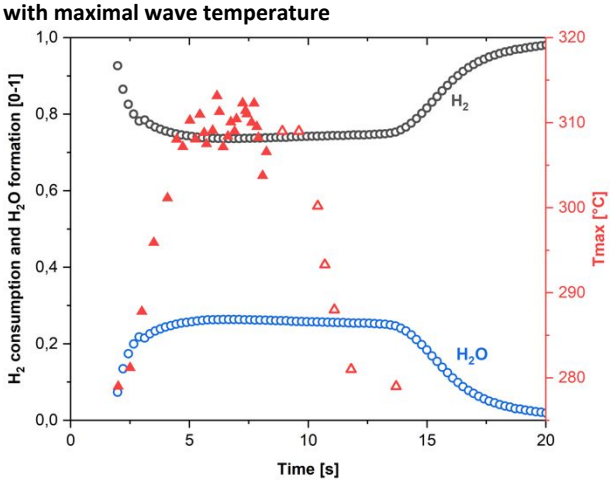

Figure 2: a) Temperature profile of the injection of 20ml/min H_2 into the He filled reaction cell. The parabolic shape in space and time indicates an accelerated reaction; b) Linear regression of the wave acceleration determined by means of five measurement points; c) Normalized water formation and hydrogen consumption overlapped with the maximal cell temperature.

4.2 H_2 and CO_2 saturated surfaces

To investigate the influence of different initial surface coverages on the reaction between H_2 and CO_2, two experiments have been carried out. Firstly, the injection of CO_2 to a H_2 filled cell and secondly, vice-versa, H_2 was injected to a CO_2 filled cell. The gas exchange reaction was investigated for volumetric flows of 5ml/min, 10ml/min and 20ml/min. The experimental results of the 10ml/min H_2 and CO_2 injections are

discussed in the following and the results at different space velocities of the 5ml/min and 20ml/min injections are given in the supporting information in sections 5.2 and 5.3.

4.2.1 CO_2 injected to an H_2 exposed catalyst

The injection of CO_2 to the H_2 filled cell results in a strongly exothermic reaction causing a thermal runaway (Figure 3a-c). The reaction front accelerates continuously from 2.2 mm/s at the beginning of the cell to 3.8mm/s towards the end of the reaction cell and the reaction hotspot increases to a maximum of 12K towards the end of the reaction cell. The parabolic shape of the reaction temperature profile is clearly visible in Figure 3b. The analysis of the MS spectra (Figure 3c) and the carbon balance reveals that in the first 2-3 seconds no CO_2 is measured at the reactor outlet, showing that CO_2 is either converted to CH_4 or adsorbed on the surface. The overlay of the maximal hotspot temperature in the reactor at a given time with the carbon balance reveals the following: After the strongly exothermic initial reaction front has moved through the cell, the rate of methane formation decreases and a quasi-steady state hotspot of approximatively 5K is established. This hotspot slowly declines as the H_2 in the cell is consumed until full depletion and stop of the reaction after approximatively 150s (out of the scale of Figure 3c).

The CO_2 adsorption on the Ru/Al_2O_3 catalyst has been investigated at elevated temperature with the aim to explain the observed delay in the CO_2 detection by MS. By means of temperature programmed desorption (TPD), it was determined that there are three major CO_2 binding modes with different activation energies of desorption on the Ru/Al_2O_3 catalyst. Upon adsorbing CO_2 on the reduced catalyst at 50°C and heating the reactor with a ramp of 10°C/min, the major CO_2 desorption peak occurred between 100-120°C, the second desorption peak was found at 390°C and the third minor peak at 510°C (Section 3.5 and 3.9 in the SI). Since the experiments in the IR-reaction cell are carried out above 280°C, the desorption mode at 100-120°C can be neglected. The activation energy of desorption of the second CO_2 binding mode at above 300°C is 109±10 kJ/mol (See Figure S10 and Table S2). Therefore, CO_2 can chemisorb on the surface above 280°C and the delay in CO_2 detection could be ascribed to the surface adsorption which was also quantified by means of a microbalance (Figure S5). It was found that 1.4±0.2mg of $CO_2/g_{Ru/Al2O3}$ can be adsorbed at 280°C which corresponds to 1.46ml of CO_2 at 280°C and ambient pressure. Therefore, at a CO_2 inflow of 10ml/min, the 172mg of Ru/Al_2O_3 catalyst would be fully CO_2 saturated in 1.5s if no reaction occurred (details on the calculation of the number of surface sites are given in SI section 3.9). The detected delay of CO_2 of 2-3 s is therefore explained by the immediate conversion of CO_2 to CH_4 due to the rapid reaction activation and due to the surface adsorption of CO_2.

The surface species formation upon injecting CO_2 has been investigated by means of DRIFTS in comparable reaction conditions (temperature and pressure) but in a different reaction cell. Therefore, the timescale of the DRIFTS results in Figure 3a is not directly comparable to the timescale in Figure 3b and Figure 3d. It was found that the formation of the reaction intermediates[29] carbon monoxide CO*, bicarbonate HCO_3^-*, and formate $HCOO^-$* starts immediately upon injecting CO_2 (See Figure S19).

4.2.2 H_2 injected to CO_2

The injection of H_2 to a CO_2 filled cell results in a significant inhibition of the reaction activation as it can be seen in Figure 3d-f. A weak local hotspot is formed at the injection point of H_2 and the analysis of the MS spectra reveals that CH_4 is formed with a low rate (Figure 3f). After approximatively 15 s, the reaction activates and the hotspot of around 5K rapidly moves through the reaction cell. No clear wave-front acceleration trend is observed. After the reaction activation, methane is formed at a constant rate for 15s

and a quasi-steady state hotspot of 3K is established before the remaining CO_2 and carbon adsorbed species are further converted to CH_4 and the hotspot slowly declines.

After 20-30s of a quasi-steady state reaction, the hotspot further declines and reaches a minimal value after 150s (out of figure scale). At this point, CO_2 is no longer detected in significant quantities in the gas phase. Surprisingly, methane is formed and detected until 400s with a declining rate. This indicates that the injected H_2 continues to react with strongly adsorbed carbon species (such as CO*) at a low reaction rate.

In DRIFTS measurements, adsorbed CO* and HCO_3^-* are detected (Figure 3d) prior to the hydrogen injection (while no formate/$HCOO^-$* was observed). Upon injecting H_2, formate was slowly formed and the CO* concentration only changed marginally (See section 6 of the SI for details on the DRIFTs analysis). The analysis of the reaction heatmap and the correlated MS spectra, surface species and carbon balance lead to the following interpretation: The surface is initially covered by carbon species, which inhibit the formation of methane. With the continuous feed of H_2, the surface is continuously reduced and methane is formed at a low rate. As soon as a critical degree of reduction is reached, the reaction rate increases starting from a localized hotspot close to the injection point of H_2.

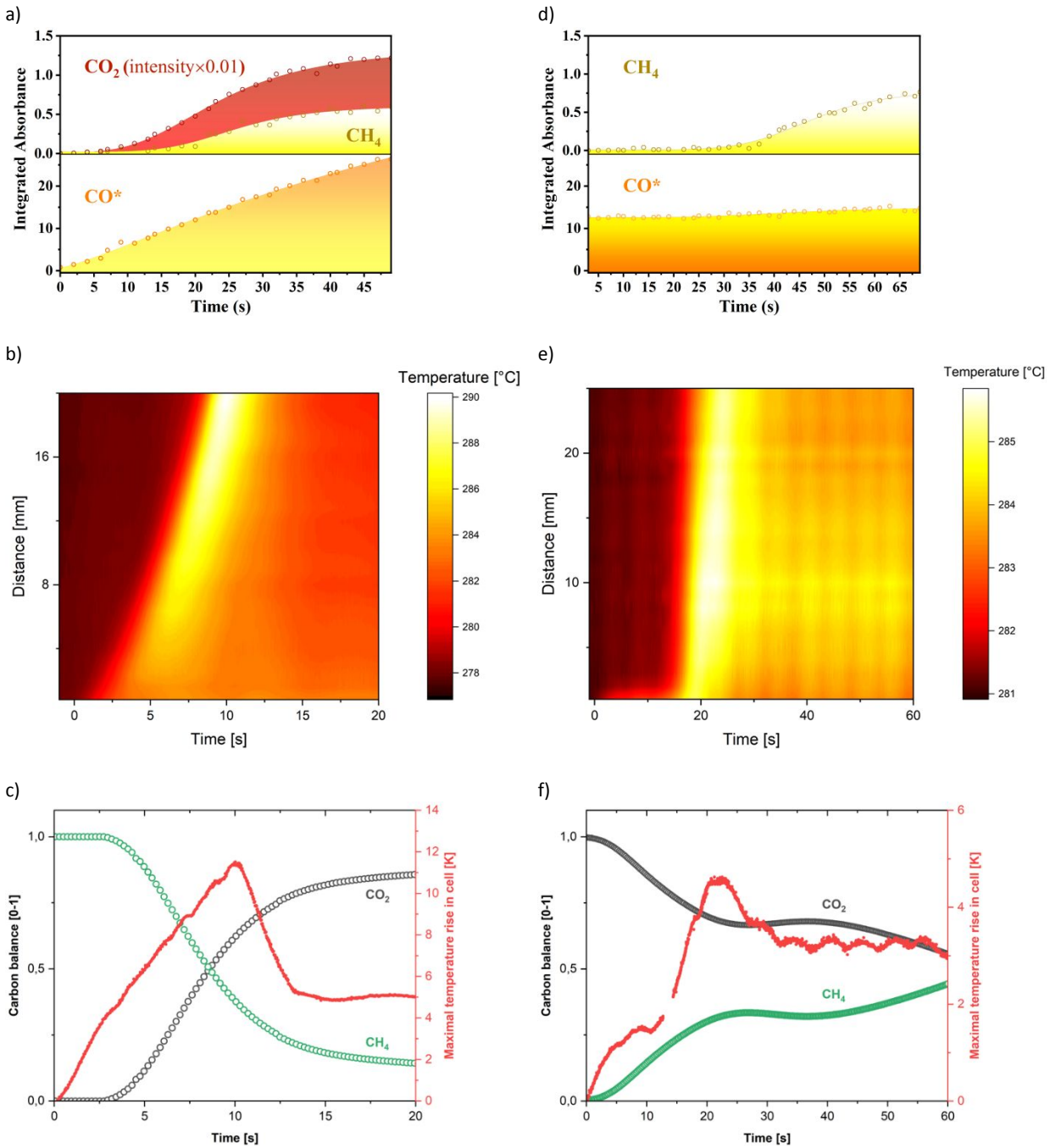

Figure 3: a) Evolution of CO_2, CH_4 and the key intermediate CO* upon injecting CO_2 to the H_2 filled DRIFTS reaction cell; b) Heatmap of CO_2 injection to H_2 filled reaction cell at 279°C; c & f) Carbon balance between the reactant CO_2 and the product CH_4 with the maximum hotspot temperature overlay; d) Evolution of CO_2, CH_4 and the key intermediate CO* upon injecting H_2 to the CO_2 filled DRIFTS reaction cell; e) Heatmap of H_2 injection to CO_2 filled reaction cell at 280°C. Note that the time axis for the DRIFTS surface investigation (a,d) is not directly comparable with the timescale of the thermography and MS experiments since they were carried out in a different reaction cell.

4.3 Sabatier reaction

The Sabatier reaction (eq. 2), where H_2 and CO_2 are injected simultaneously to the He filled reaction cell, has been investigated in different reaction conditions.

$$CO_2 + 4H_2 \rightleftharpoons CH_4 + 2H_2O \qquad \Delta H_R = -164.9 \frac{kJ}{mol} \tag{2}$$

At first, the reaction was analysed at different space velocities (5, 10 and 20 ml/min volumetric inflow) injecting the reactants to a He filled cell. Secondly, the Sabatier reaction was analysed at different He dilutions where the injected gas was composed the reactants (H_2 and CO_2) and 25%, 50% and 75% of He, respectively. The combined thermal and composition analysis of the Sabatier reaction reveals interesting correlations between the thermal profile in the cell, the maximal reaction hotspot, the maximal CO_2 conversion and gas retention times.

Figure 4 shows the heat profile in the middle line of the cell, resolved in time and space, revealing the activation and the steady state temperature profile for the injection of H_2, CO_2 in a 4:1 ratio diluted with 25% He to the He filled reaction cell. This example is representative for the investigation of the Sabatier reaction in different conditions since it shows the continuously accelerated pre-activation reaction front, the main activation reaction front with the highest exothermicity and the steady-state hotspot, established after the reaction is activated. The results of these investigations are discussed in detail in the following.

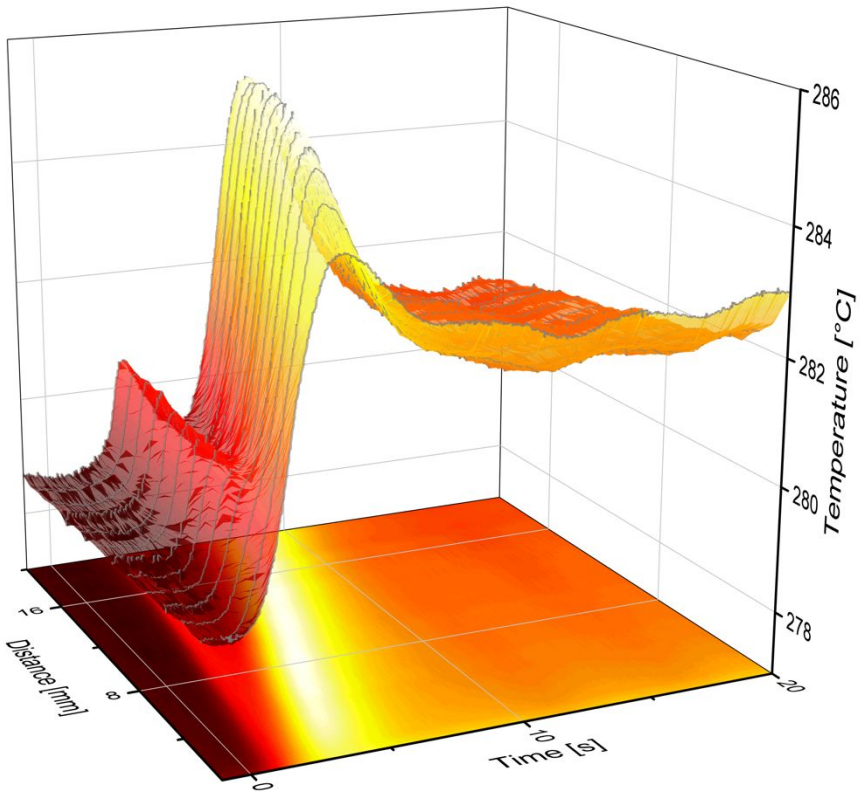

Figure 4: Temperature profile for the Sabatier reaction with 25% He dilution. The main reaction activation follows a continuously accelerated initial reaction front. At steady state the temperature profile shows a gradient between the inlet and outlet.

4.3.1 Influence of space velocities

The Sabatier reaction was investigated at different space velocities (Figure 5). It was found that a continuously accelerated reaction front goes through the cell prior to a second activation front. The second reaction front moves through the reactor with approximatively constant velocity, in contrast to the continuously accelerated initial front (See Figure S16, Table S6). After the major reaction peak, the hotspot declines to a lower steady-state value originated by the established surface reaction rate. The hotspot intensity for the flow of 5ml/min and 10ml/min is concentrated on the first half of the reactor, where the concentration of reactant is high and consequently the reaction rate is elevated. For the 20ml/min flow the maximal hotspot is pushed further back due to the higher space velocity. The steady state hotspot is established after 12s for the injection of 20ml/min, 27s for 10ml/min injection up to 60s for the 5ml/min injection. In all cases, the steady state hotspot exhibits a weak gradient from the injection point towards the reactor outlet of approximatively 1-2K due to the decreasing reactant concentration along the reaction axis.

The interpretation for the continuously accelerated fast initial reaction front is that the injected reactants react rapidly on the free catalysts surface sites, but the strongly diluted He environment hinders a further development of the reaction. Indeed, the initial rate is apparently faster than the transport of the reactants to the surface (in the initially He diluted environment) to maintain the initial reaction kinetics (this phenomenon is further discussed in section 4.3.2 on the basis of the He diluted injections). Only after a critical reactant concentration is achieved on the surface, the Sabatier reaction fully activates and goes

through a maximal hotspot prior to reaching a steady state. The CO_2 conversion in steady state is between 0.88 and 0.82 for the injection at 5 and 10ml/min, but it is significantly lower for the highest injection volume at 20ml/min, reaching a value of 0.51 (Table S7). This is explained by the higher residence time at the lower space velocities allowing the reactants more time to react on the surface. The lower conversion at high space velocity can be correlated with the position of the hotspot: The high temperature region at 20ml/min is more uniformly distributed through the cell and furthermore reaches the maximum towards the end of the cell[30]. This indicates that the convective transport of reactants is not rate limiting, but the system is controlled by the kinetics of the surface reaction.

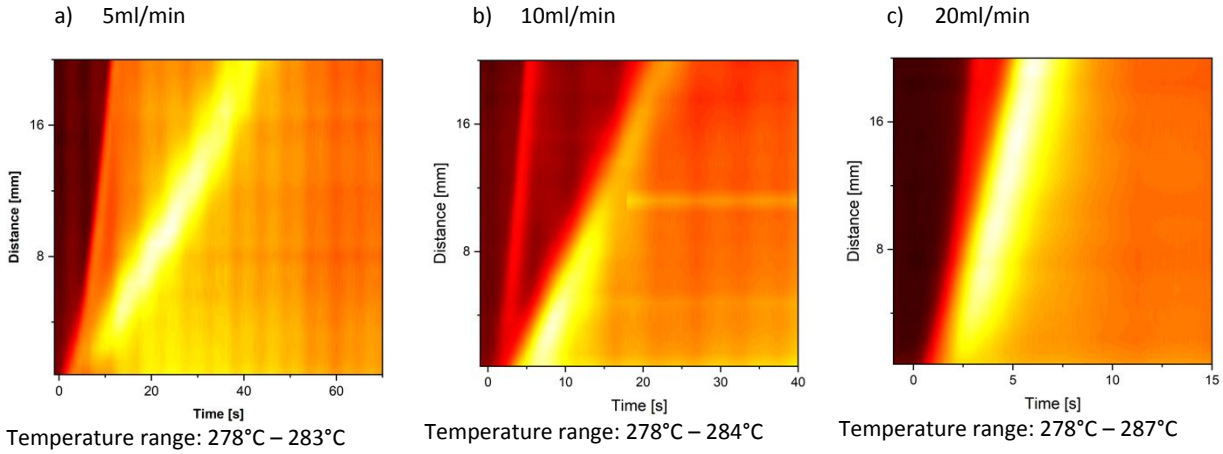

Figure 5: Sabatier reaction activation at different space velocities. The reaction cell is initially filled with He before H_2 and CO_2 are injected. The deviation between the pre-activation reaction front and the main reaction activation front is reduced with increasing space velocity (from a-c).

4.3.2 He diluted Sabatier reaction

The analysis of the Sabatier reaction at different He dilutions by means of IR-thermography and MS reveals that the hotspot intensity and evolution strongly depend on the He dilution (Figure 6a-b, Figure S17). The intensity of the maximal hotspot decreases from approximatively 9K for the undiluted injection to 2K for the 75% He diluted Sabatier reaction.

Furthermore, the initial reaction activation front deviates more from the main activation front with increasing He dilution (Figure 6a, Figure S19). The position of the maximal hotspot migrates towards the injection point with increasing He dilution. The CO_2 conversion is correlated to the hotspot migration and increases from 0.51 for the undiluted reactants injection at 20ml/min to 0.82 for the 75% He diluted injection, values that can be correlated to the effect of space velocity (for the reactants) discussed in the previous section. The hotspot intensity is decreased since the concentration of reactants per catalyst site is reduced (Figure 6b).

An additional observed phenomenon is the increase in CO_2 and H_2O delay at the reactor outlet with increasing He dilution as observed by means of MS (Table 3 below, Figure S18). In order to explain the delayed detection of CO_2, the adsorption was estimated for the different He dilutions. As already discussed in section 4.2.1, 1.4±0.2mg of $CO_2/g_{Ru/Al2O3}$ can be adsorbed at 280°C. This means that $5.5x10^{-6}$ mols of CO_2 can be adsorbed on 172mg of catalyst. The delay in CO_2 detection at the reactor outlet can

be explained by the reduced molar inflow of CO_2 and H_2 with higher He dilutions, the surface adsorption (more surface sites per injected reactant) and the increasing conversion with higher He dilution.

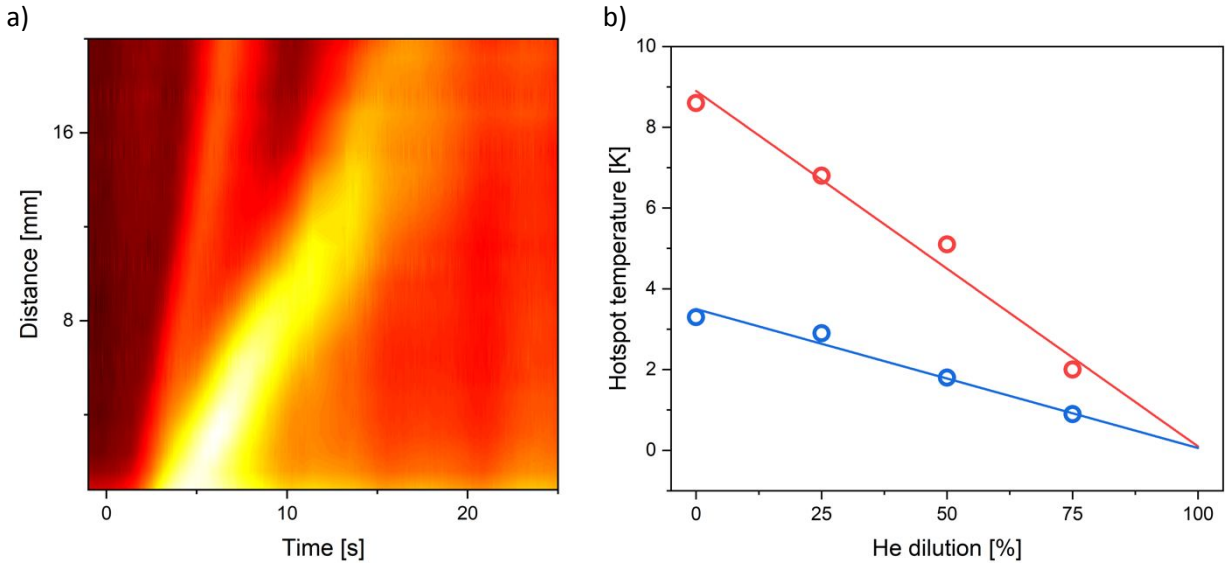

Figure 6: a) The hotspot intensity at 75% He dilution for the Sabatier reaction is concentrated to the injection point while the hotspot position is pushed further backwards in the reaction cell with increasing reactants concentration (See Table 3). The temperature range of the heatmap from dark red to white corresponds to 279°C to 282°C. b) Decrease of maximal and steady-state hotspot intensity with increasing He dilution in the Sabatier reaction.

Table 3: Comparison of selected parameters for the reactants' injection of the Sabatier reaction at 20ml/min to the He filled reaction cell at different He dilutions.

He dilution [%]	**Maximal hotspot intensity [K]**	**Steady state hotspot intensity [K]**	**Position of maximal hotspot [mm]**	**v_{max} initial wave front [mm/s]**	**CO_2 conversion at steady state [0-1]**	**Molar CO_2 inflow [mol/s]x10^{-6}**	**Estimated CO_2 retention time [s]**	**CO_2 retention time [s]**
0	8.6	3.3	15	12.2	0.51	3.4	3-7	4
25	6.8	2.9	7	12.2	0.62	2.5	5-11	9
50	5.1	1.8	3	12.2	0.68	1.7	7-20	15
75	2	0.9	0	5.8	0.82	0.8	24-38	35

5. Conclusion and Outlook

In this work we investigated the reaction between H_2 and CO_2 on a 2% Ru/Al_2O_3 catalyst by means of operando infrared thermography, rapid and quantitative mass spectrometry and diffuse reflectance infrared Fourier transform spectroscopy. Besides the surface reduction analysis of the oxidized catalyst surface and gas exchange reactions between CO_2 and H_2, the Sabatier reaction was investigated under different reaction conditions and He dilutions. New insights on the reaction activation behavior were presented and it was shown that the initial surface conditions have a determining influence on the reaction activation. In a hydrogen-rich environment, the thermal runaway of the reaction front was observed and the front accelerated continuously from the injection point to the outlet. Adsorbed carbon surface species significantly inhibit the reaction activation and a local hotspot at the injection point is formed until the surface is sufficiently reduced and methane can be formed throughout the reaction cell. The He dilution of the reactant gases in the Sabatier reaction causes a dislocation of the maximal activation hotspot and it alters its intensity. Furthermore, a continuously accelerated pre-reaction activation front was observed if the reactants of the Sabatier reaction are injected to the He filled reaction cell: The initial reaction activation cannot be maintained due to the high initial dilution and the mass transport of reactants to the catalyst surface becomes rate limiting.

The described methodology in the dedicated reaction cell can be applied to any endo or exothermic reaction. It is of particular interest for exothermic reactions such as the Sabatier, Fischer-Tropsch or the Haber-Bosch process for which the described reaction cell can serve as a model system to gain an in depth understanding of transient reaction properties which can lead to the advanced design of reactors which operate in unsteady state conditions and go through numerous activation and deactivation cycles.

6. Acknowledgement

Financial support by the Swiss National Science Foundation: Project "Investigation and modeling of new CO_2 adsorption materials and their interaction with hydrogen" Verfügung 200021_163010/1 and the SCCER Heat & Electricity Storage (innosuisse) are acknowledged. Jérémie Berard is acknowledged for his reactor design propositions and drawings. Furthermore, we are thankful to Stéphane Voeffray and Robin Délèze for the constructive discussions on the reactor design and for manufacturing the reactor.

7. Supplementary information

The Supporting Information is available free of charge on the ACS Publications website and contains: details on the experimental setup, further catalysts characterisation, supplementary experimental results, details on the DRIFTS experiments.

8. References

(1) Ring, F. J. Pioneering Progress in Infrared Imaging in Medicine. *Quant. Infrared Thermogr. J.* **2014**, *11* (1), 57–65. https://doi.org/10.1080/17686733.2014.892667.

(2) Holzwarth, A.; Schmidt, H. W.; Maier, W. F. Detection of Catalytic Activity in Combinatorial Libraries of Heterogeneous Catalysts by IR Thermography. *Angew. Chemie - Int. Ed.* **1998**, *37* (19), 2644–2647. https://doi.org/10.1002/(SICI)1521-3773(19981016)37:19<2644::AID-ANIE2644>3.0.CO;2-#.

(3) Krämer, M.; Duisberg, M.; Stöwe, K.; Maier, W. F. Highly Selective CO Methanation Catalysts for the Purification of Hydrogen-Rich Gas Mixtures. *J. Catal.* **2007**, *251* (2), 410–422. https://doi.org/10.1016/j.jcat.2007.07.030.

(4) Moates, F. C.; Somani, M.; Annamalai, J.; Richardson, J. T.; Luss, D.; Willson, R. C. Infrared Thermographic Screening of Combinatorial Libraries of Heterogeneous Catalysts. *Ind. Eng. Chem. Res.* **1996**, *35* (12), 4801–4803. https://doi.org/10.1021/ie960476k.

(5) Loskyll, J.; Stoewe, K.; Maier, W. F. Infrared Thermography as a High-Throughput Tool in Catalysis Research. *ACS Comb. Sci.* **2012**, *14* (5), 295–303. https://doi.org/10.1021/co200168s.

(6) Zech, T.; Bohner, G.; Laus, O.; Klein, J.; Fischer, M. Design, Fabrication, and Application of a Massively Parallel Single-Bead Microreactor System for High-Throughput Experimentation in Heterogeneous Catalysis. *Rev. Sci. Instrum.* **2005**, *76* (6). https://doi.org/10.1063/1.1906088.

(7) Kopyscinski, J.; Schildhauer, T. J.; Vogel, F.; Biollaz, S. M. A.; Wokaun, A. Applying Spatially Resolved Concentration and Temperature Measurements in a Catalytic Plate Reactor for the Kinetic Study of CO Methanation. *J. Catal.* **2010**, *271* (2), 262–279. https://doi.org/10.1016/j.jcat.2010.02.008.

(8) Lalinde, J. A. H.; Jiang, J.; Jai, G.; Kopyscinski, J. Preparation and Characterization of Ni/Al2O3 Catalyst Coatings on FeCrAl-Loy Plates Used in a Catalytic Channel Reactor with in-Situ Spatial Profiling to Study CO2 Methanation. *Chemical Engineering Journal*. 2018. https://doi.org/10.1016/j.cej.2018.09.161.

(9) Techniques, S. M. Improved Kinetic Data Acquisition Using An Optically Accessible Catalytic Plate Reactor with Spatially-Resolved Measurement Techniques. Case of Study: CO2 Methanation. *Catalysts* **2018**, *8* (2), 86. https://doi.org/10.3390/catal8020086.

(10) Schüler, C.; Wolf, M.; Hinrichsen, O. Contactless Temperature Measurements under Static and Dynamic Reaction Conditions in a Single-Pass Fixed Bed Reactor for CO 2 Methanation. *J. CO2 Util.* **2018**, *25* (March), 158–169. https://doi.org/10.1016/j.jcou.2018.03.016.

(11) Frey, M.; Romero, T.; Roger, A. C.; Edouard, D. An Intensification of the CO2 Methanation Reaction: Effect of Carbon Nanofiber Network on the Hydrodynamic, Thermal and Catalytic Properties of Reactors Filled with Open Cell Foams. *Chem. Eng. Sci.* **2019**, *195*, 271–280. https://doi.org/10.1016/j.ces.2018.11.028.

(12) Frey, M.; Romero, T.; Roger, A. C.; Edouard, D. Open Cell Foam Catalysts for CO2 Methanation: Presentation of Coating Procedures and in Situ Exothermicity Reaction Study by Infrared Thermography. *Catal. Today* **2016**, *273*, 83–90. https://doi.org/10.1016/j.cattod.2016.03.016.

(13) Jolly, J.; Pavageau, B.; Tatibouët, J.-M. Time-Resolved IR Thermographic Detection of Gaseous Molecules Adsorption on Oxide Supports. *Quant. Infrared Thermogr. J.* **2011**, *8* (2), 129–137. https://doi.org/10.3166/qirt.8.129-137.

(14) Zhang, J. S.; Zhang, C. Y.; Liu, G. T.; Luo, G. S. Measuring Enthalpy of Fast Exothermal Reaction with Infrared Thermography in a Microreactor. *Chem. Eng. J.* **2016**, *295*, 384–390. https://doi.org/10.1016/j.cej.2016.01.100.

(15) Barin, J. S.; Tischer, B.; Oliveira, A. S.; Wagner, R.; Costa, A. Ben; Flores, E. M. M. Infrared Thermal Imaging: A Tool for Simple, Simultaneous, and High-Throughput Enthalpimetric Analysis. *Anal. Chem.* **2015**, *87* (24), 12065–12070. https://doi.org/10.1021/acs.analchem.5b02753.

(16) Luss, D.; Marwaha, B. Hot Zones Evolution and Dynamics in Heterogeneous Catalytic Systems. *Chaos* **2002**, *12* (1), 172–181. https://doi.org/10.1063/1.1448808.

(17) Qin, F.; Wolf, E. E.; Engineering, C.; Dame, N.; Dame, N. CATALYSTS. **1995**, *49* (24), 4263–4267.

(18) Haber, J.; Kashid, M. N.; Borhani, N.; Thome, J.; Krtschil, U.; Renken, A.; Kiwi-Minsker, L. Infrared Imaging of Temperature Profiles in Microreactors for Fast and Exothermic Reactions. *Chem. Eng. J.* **2013**, *214*, 97–105. https://doi.org/10.1016/j.cej.2012.10.021.

(19) Ramirez, A.; Hueso, J. L.; Mallada, R.; Santamaria, J. In Situ Temperature Measurements in Microwave-Heated Gas-Solid Catalytic Systems. Detection of Hot Spots and Solid-Fluid Temperature Gradients in the Ethylene Epoxidation Reaction. *Chemical Engineering Journal*. 2017, pp 50–60. https://doi.org/10.1016/j.cej.2017.01.077.

(20) Mutschler, R.; Luo, W.; Moioli, E.; Züttel, A. Fast Real Time and Quantitative Gas Analysis Method for the Investigation of the CO2 Reduction Reaction Mechanism. *Rev. Sci. Instrum.* **2018**, *89*, 114102.

(21) Falbo, L.; Martinelli, M.; Visconti, C. G.; Lietti, L.; Bassano, C.; Deiana, P. Kinetics of CO2methanation on a Ru-Based Catalyst at Process Conditions Relevant for Power-to-Gas Applications. *Appl. Catal. B Environ.* **2018**, *225* (November 2017), 354–363. https://doi.org/10.1016/j.apcatb.2017.11.066.

(22) Mutschler, R.; Moioli, E.; Luo, W.; Gallandat, N.; Züttel, A. CO2hydrogenation Reaction over Pristine Fe, Co, Ni, Cu and Al2O3supported Ru: Comparison and Determination of the Activation Energies. *J. Catal.* **2018**, *375*, 139–149. https://doi.org/10.1016/j.jcat.2018.08.002.

(23) Gallandat, N.; Mutschler, R.; Vernay, V.; Yang, H.; Züttel, A. Experimental Performance Investigation of a 2 KW Methanation Reactor. *Sustain. Energy Fuels* **2018**, *2* (5), 1101–1110. https://doi.org/10.1039/C8SE00073E.

(24) Weatherbee, G. D.; Bartholomew, C. H. Hydrogenation of CO2 on Group VIII Metals. IV. Specific Activities and Selectivities of Silica-Supported Co, Fe, and Ru. *J. Catal.* **1984**, *87* (2), 352–362. https://doi.org/10.1016/0021-9517(84)90196-9.

(25) Moioli, E.; Gallandat, N.; Züttel, A. Parametric Sensitivity in the Sabatier Reaction over Ru/Al2O3 – Theoretical Determination of the Minimal Requirements for Reactor Activation. *React. Chem. Eng.* **2018**. https://doi.org/10.1039/C8RE00133B.

(26) Porta, A.; Falbo, L.; Visconti, C. G.; Lietti, L.; Bassano, C.; Deiana, P. Synthesis of Ru-Based Catalysts for CO 2 Methanation and Experimental Assessment of Intraporous Transport

Limitations. *Catal. Today* **2019**, No. October 2018. https://doi.org/10.1016/j.cattod.2019.01.042.

(27) Madey, T.; Engelhardt, A.; Menzel, D. Adsorption of Oxygen and Oxydation of CO on the Rutheium (001) Surface. *Surf. Sci.* **1975**, *48*, 304–328.

(28) Iwamoto, M.; Yoda, Y.; Yamazoe, N.; Seiyama, T. Study of Metal Oxide Catalysts by Temperature Programmed Desorption. 4. Oxygen Adsorption on Various Metal Oxides. *J. Phys. Chem.* **1978**, *82* (24), 2564–2570. https://doi.org/10.1021/j100513a006.

(29) Zhao, K.; Wang, L.; Calizzi, M.; Moioli, E.; Zuttel, A. In Situ Control of the Adsorption Species in CO 2 Hydrogenation: Determination of Intermediates and Byproducts. *J. Phys. Chem. C* **2018**, *122*, 20888–20893. https://doi.org/10.1021/acs.jpcc.8b06508.

(30) Moioli, E.; Gallandat, N.; Züttel, A. Model Based Determination of the Optimal Reactor Concept for Sabatier Reaction in Small-Scale Applications over Ru/Al2O3. *Chem. Eng. J.* **2019**, *375*, 121954. https://doi.org/10.1016/j.cej.2019.121954.

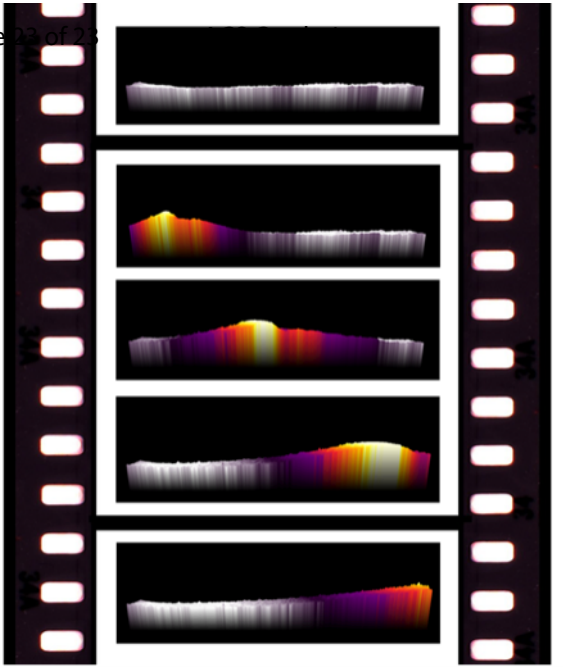

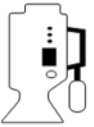

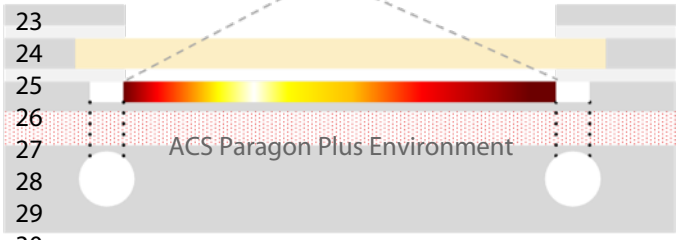
ACS Paragon Plus Environment